H-scan sensitivity to scattering size

Mawia Khairalseed,[a,b] Kenneth Hoyt,[a,c] Juvenal Ormachea,[d] Alberto Terrazas,[e] and Kevin J. Parker[d,*]
[a]University of Texas at Dallas, Department of Bioengineering, Richardson, Texas, United States
[b]Sudan University of Science and Technology, Department of Biomedical Engineering, Khartoum, Sudan
[c]University of Texas Southwestern Medical Center, Department of Radiology, Dallas, Texas, United States
[d]University of Rochester, Department of Electrical and Computer Engineering, Rochester, New York, United States
[e]Tecnológico de Monterrey, Grupo de Bioinformatica, Monterrey, Nuevo León, Mexico

Abstract. In the H-scan analysis and display, visualization of different scattering sizes and types is enabled by a matched filter approach involving different orders of Gaussian weighted Hermite functions. An important question with respect to clinical applications involves the change in H-scan outputs with respect to small changes in scatterer sizes. The sensitivity of H-scan outputs is analyzed using the theory of backscatter from a compressible sphere. Experimental corroboration is established using mono dispersed spherical scatterers in phantoms. With a 6-MHz center frequency broadband transducer, it is possible to visualize changes in scattering size in the order of 10 to 15 μm in phantoms and also changes in *ex vivo* bovine liver tissue due to edema caused by hypotonic perfusion. [DOI: 10.1117/1.JMI.4.4.043501]

Keywords: ultrasound; scattering; Rayleigh scattering; tissue characterization.

Paper 17214R received Jul. 13, 2017; accepted for publication Oct. 12, 2017; published online Nov. 6, 2017.

1 Introduction

The H-scan analysis links the mathematics of Gaussian weighted Hermite (GWH) functions to the physics of scattering and reflections from different objects within a standard convolution model of pulse-echo systems.[1,2] Specific integer orders, termed $\mathbf{G}Hn$, are related to the n'th derivative of a Gaussian function.[3,4] Matched filters employing specific orders of $\mathbf{G}Hn$ functions are used to analyze the content of echoes and to colorize the display, providing visual discrimination between scattering and reflecting types.

Previous works have studied phantoms and tissues where resulting H-scan colors could be linked to scattering types and sizes. An important related issue is the sensitivity of H-scan analysis to small changes in scattering sizes, down to cellular level diameters, such as 8 to 10 μm for red blood cells. Cell sizes and vascular diameters can vary in tissue in response to a number of factors, including inflammation, edema, injury, and various pathological processes. In these cases, the detection of small changes in scattering sizes and visualization of the resulting changes in scattering properties is a longstanding goal in medical ultrasound.[5–10] The H-scan analysis represents a distinct approach tied to the properties of the GWH functions, and the sensitivities of these are analyzed theoretically in Sec. 2. Experimental confirmations in phantoms and in beef liver sections exposed to hypotonic solution are given in Sec. 3.

2 Theory

The scattering of acoustic waves from inhomogeneities has a long history.[11,12] In this section, we examine the backscattered pressure from an inhomogeneity of compressibility. In this derivation, we follow the classical approach described in Chapter 8 of Morse and Ingard.[13] In this treatment, under the Born approximation (weak scatterers) with an incident plane wave P_i of frequency ω traveling in the x-direction

$$P_i = A\mathbf{e}^{ikx}, \tag{1}$$

where A is the amplitude, $k = \omega/c$ is the wavenumber, and c is the speed of sound. Then, the backscattered pressure P_{bs} is approximately

$$P_{\mathrm{bs}}(k,x) \cong A\left(\frac{\mathbf{e}^{ikx}}{x}\right)\phi_s(k), \tag{2}$$

where

$$\phi_s(k) = (k)^2\left(\frac{1}{4\pi}\right)\int\int\int \kappa(r)\mathbf{e}^{i2\hat{\mathbf{k}}\cdot\hat{\mathbf{r}}}dVol, \tag{3}$$

where $\kappa(r)$ is the (small) fractional change in compressibility within the scatterer, the $2\hat{k}$ term in the complex exponential comes from the 180 deg direction of backscatter, and the integration is over the scattering volume. This equation has the form of a spatial Fourier transform of the scatterer. Here, we assume an isotropic spherical $\kappa(r)$ and utilize spherical coordinates where the polar angle θ is aligned with the x-axis coordinate system, and $\hat{\mathbf{k}}$ is oriented along the x-axis. Then $\hat{\mathbf{k}}\cdot\hat{\mathbf{r}} = kr\cos\theta$, $dVol = r^2\sin\theta d\theta d\phi$, and

$$\int\int\int \kappa(r)e^{i2\hat{\mathbf{k}}\cdot\hat{\mathbf{r}}}dVol = \int_{r=0}^{\infty}\int_{\theta=0}^{\pi}\int_{\phi=0}^{2\pi}\kappa(r)\mathbf{e}^{i2kr\cos\theta}r^2\sin\theta\mathrm{d}\theta\mathrm{d}\phi. \tag{4}$$

Integrating first over ϕ then θ yields

$$= \left(\frac{2\pi}{k}\right)\int_{r=0}^{\infty} r\cdot\kappa(r)\cdot\sin(2kr)\mathrm{d}r, \tag{5}$$

*Address all correspondence to: Kevin J. Parker, E-mail: kevin.parker@rochester.edu

2329-4302/2017/$25.00 © 2017 SPIE

and assuming a uniform sphere of $\kappa(r) = \kappa_0$ $(0 \le r \le a)$ and zero elsewhere, the integral yields

$$= \kappa_0 4\pi a^3 \left(\frac{j_1(2ka)}{2ka}\right), \tag{6}$$

where $j_1(x)$ is a spherical Bessel function of order 1^3. Finally, incorporating all terms from Eq. (2)

$$P_{\mathrm{bs}}(k,x) \cong A_1 \kappa_0 \left(\frac{\mathbf{e}^{ikx}}{x}\right)(k^2)(a^3)\left(\frac{j_1(2\ ka)}{2\ ka}\right), \tag{7}$$

and in the long wavelength limit as $ka \to 0$, the $j_1(2ka)/2ka$ term approaches a constant (1/3), and we have the classical Rayleigh scattering proportional to k^2 and a^3 as shown in Eq. (8.1.21) of Morse and Ingard.[13] The Rayleigh limit is important in the H-scan analysis since the k^2 (or ω^2) frequency transfer function will convert a $\mathbf{G}H4$ pulse to a $\mathbf{G}H6$ echo.[1,2] A similar result involving the $j_1(2ka)/2ka$ form factor is also well established for ensemble-averaged differential cross-section backscatter coefficients for randomly positional spheres in a medium,[14,15] albeit with k^4a^6 factors related to measures of integrity.

Next, assuming a convolution model of pulse-echo imaging of this scatterer,[1,2,16,17] we assume a $\mathbf{G}H4$ pulse is transmitted and backscattered by the scatterer via Eq. (7) and then is received and convolved with a $\mathbf{G}Hn$ matched filter, where in this discussion for simplicity, n is restricted to even integers such as $\mathbf{G}H2$, $\mathbf{G}H4$, $\mathbf{G}H6$, and $\mathbf{G}H8$. Thus, the echo $\mathbf{e}(t)$ formation model is

$$\mathbf{e}(t) = TR(t) * bs(t) * \mathbf{G}Hn\left(\frac{t}{\tau}\right), \tag{8}$$

where the asterisk symbol implies convolution and $TR(t)$ is the round-trip impulse response of the transducer, assumed to be $\mathbf{G}H4(t/\tau)$. Furthermore, $bs(t)$ is the impulse response of the scatterer and $\mathbf{G}H4(t/\tau)$ is the H-scan channel filter assigned to a color. The Fourier transform of $\mathbf{e}(t)$ is given by the product of the respective component transforms

$$E(\omega) = \Im\left[\mathbf{G}H4\left(\frac{t}{\tau}\right)\right] * P_{\mathrm{bs}}\left(k = \frac{\omega}{c}\right) * \Im\left[\mathbf{G}Hn\left(\frac{t}{\tau}\right)\right], \tag{9}$$

where P_{bs} is defined by Eq. (7) and $\mathbf{e}(t)$ is the Fourier transform of $E(\omega)$

$$\mathbf{e}(t) = \int_{-\infty}^{\infty} E(\omega)\mathbf{e}^{j\omega t}\mathrm{d}\omega. \tag{10}$$

Assuming x is chosen to produce a zero phase system and the maximum value of $\mathbf{e}(t)$ is denoted as $\mathbf{e}_{\max}$, occurring at $t = 0$, then

$$\mathbf{e}_{\max} = \mathbf{e}(0) = \int_{-\infty}^{\infty} E(\omega)\mathrm{d}\omega. \tag{11}$$

For example, the $\mathbf{G}H2$ function is defined as

$$\mathbf{G}H2\left(\frac{t}{\tau}\right) = \mathbf{e}^{-\left(\frac{t}{\tau}\right)^2}\left[4\left(\frac{t}{\tau}\right)^2 - 2\right], \tag{12}$$

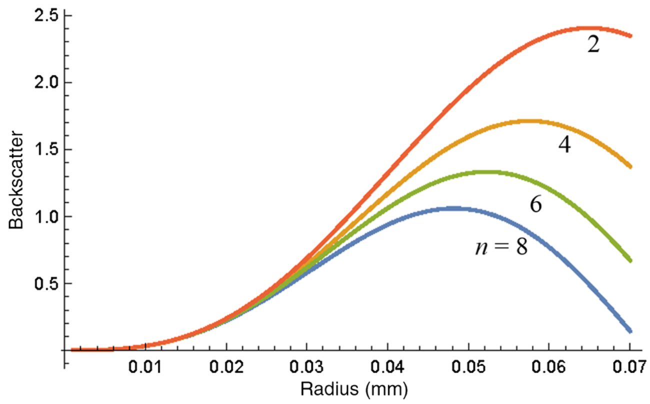

Fig. 1 The maximum echo amplitude (arbitrary units) as a function of scatterer radius, for four different matched filters: $\mathbf{G}H2$, $\mathbf{G}H4$, $\mathbf{G}H6$, and $\mathbf{G}H8$ utilized in the H-scan analysis. The examples assume that a round-trip $\mathbf{G}H4$ impulse response of a transducer is employed, set for a peak frequency of 6 MHz. A simple spherical compressibility scatterer with radius a is present in water. All four channel outputs have been normalized to equal amplitude at $a = 5$ μm for comparison. The different channels, employing different Hermite orders as matched filters, display diverging outputs as a exceeds 20 μm, and these different outputs would be visualized as color shifts in the H-scan image. In these examples, $ka = 1$ occurs at $a = 0.04$ mm. Higher frequency transducers would have similar results but shifted to lower values of a (smaller scatterers).

and the Fourier transform of $\mathbf{G}H2(t/\tau)$ is

$$\Im\left[\mathbf{G}H2\left(\frac{t}{\tau}\right)\right] = \frac{\mathbf{e}^{-\frac{1}{4}\tau^2\omega^2}\tau^3\omega^2}{\sqrt{2}}, \tag{13}$$

and in general

$$\Im\left[\mathbf{G}Hn\left(\frac{t}{\tau}\right)\right] = \frac{\mathbf{e}^{-\frac{1}{4}\tau^2\omega^2}\tau^{n+1}\omega^n}{\sqrt{2}} \quad \text{for } n \in \text{even integers.} \tag{14}$$

Then, the combination of transmit, scatter, receive, and convolve with a $\mathbf{G}H2$ matched filter can be expressed as

$$\begin{aligned}\mathbf{e}_{\max} &= A_2 \int_{\omega=0}^{\infty}\left(\frac{\mathbf{e}^{-\frac{1}{4}\tau^2\omega^2}\tau^5\omega^4}{\sqrt{2}}\right)\left[\frac{a^3\left(\frac{\omega}{c}\right)^2 j_1\left(\frac{2\omega a}{c}\right)}{\frac{2\omega a}{c}}\right] \\ &\quad \times \left(-\frac{\mathbf{e}^{-\frac{1}{4}\tau^2\omega^2}\tau^3\omega^2}{\sqrt{2}}\right)\mathrm{d}\omega \\ &= A_2 \frac{a^3 e^{-\frac{2a^2}{c^2\tau^2}}\sqrt{2\pi}\tau\left(4a^4 - 14a^2c^2\tau^2 + \frac{35c^4\tau^4}{4}\right)}{c^6\tau^6}.\end{aligned} \tag{15}$$

Similar expressions can be derived for other $\mathbf{G}Hn$ convolutions, such that the maximum echo amplitude for each H-scan channel is computed as a function of scatter radius a and transducer center frequency $\approx 1/\tau$. Results for a 6-MHz peak frequency $\mathbf{G}H4$ pulse versus scatterer radius and $\mathbf{G}Hn$ postprocessing are shown in Fig. 1.

3 Methods

A series of soft tissue-mimicking ultrasound test phantoms were used to test H-scan imaging of different sized scatterer distributions. Homogenous phantom materials were prepared by heating

10% gelatin (300 Bloom, Sigma-Aldrich, St. Louis, Missouri) in degassed water solution to 45°C.[18] Either silica (0.4%, US Silica, Pacific, Missouri) or polyethylene (0.2%, CoSpheric LLC, Santa Barbara, California) microspheres were slowly introduced during constant stirring. The silica microspheres were either 15, 30, 40, 45, or 70 μm in diameter, whereas the polyethylene microspheres were larger and 90 μm in size. All gelatin blocks were placed in a 4°C refrigerator and allowed to cool for at least 12 h before use. A heterogeneous phantom material was constructed by introducing a gelatin inclusion containing the larger microspheres (30 μm) into an otherwise homogeneous phantom block made using the smaller acoustic scatterers (15 μm). The concentration of small scatterers (15 μm) was 2%, but the large scatterers (30 μm) were 0.25% within the inclusion. Phantom scans were obtained with flash (plane wave) transmit and dynamic receive, compounded over five angles.[19]

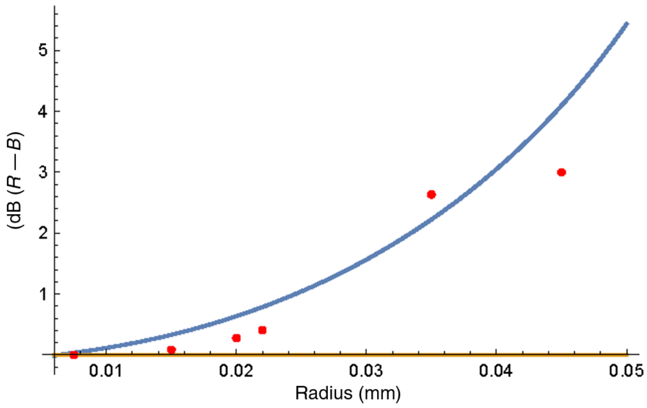

Fig. 2 Theoretical curve (solid line) showing dB difference between peak red **G**$H2$ channel and blue **G**$H8$ channel versus scatterer radius assuming a system with a 6-MHz spectral peak. Dots show experimental data where the dB difference between the average amplitude of the **G**$H2$ and the **G**$H8$ systems is shown for spherical scatterers in gelatin imaged with an ~6-MHz peak frequency broadband transducer. These differences in output between the red and blue channels change the resulting color patterns of the displayed image and enhance the visibility of shifts in scattering size.

For liver experiments, fresh veal livers were obtained directly from a local abattoir and were placed on ice and taken directly to our laboratory. There, cubes of ~3 cm in length were cut from the main lobe and placed in degassed distilled chilled water that was either an isotonic solution (0.9% NaCl added) or a hypotonic solution (0.65% NaCl). The cubes were stored at 1.5 °C for 24 h, at which time they were scanned with a Verasonics system (Verasonics, Inc., Kirkland, Washington) with a 6-MHz center frequency broadband linear array. Liver scans were obtained with a single-focal depth transmit and dynamic receive. Volume measurements were confirmed using calipers and by water displacement before and after the 24-h soaking. H-scan processing was accomplished by postprocessing the received beamformed RF echoes using **G**$H2$ and **G**$H8$ filters as described by Parker.[1,2]

4 Results

For spherical scatterers suspended in gelatin, a shift toward a relative increase in red (**G**$H2$) component was seen with increasing scattering size. Experimental data (average R – average B, each in dB) are plotted against theoretical results in Fig. 2, and example B-scan and corresponding H-scan results are shown in Fig. 3. As an example of inherent contrast, an embedded lesion is shown in Fig. 4, demonstrating a color shift in the lesion due to its composition with larger scatterers as compared with the background. The envelope statistics for the speckle and the envelope of the **G**$H2$ (red) and **G**$H8$ (blue) outputs appeared to be similar to the Rayleigh probability density function, with a ratio of mean to standard deviation (signal-to-noise ratio) of ~1.9.[20,21] For regions of interest larger

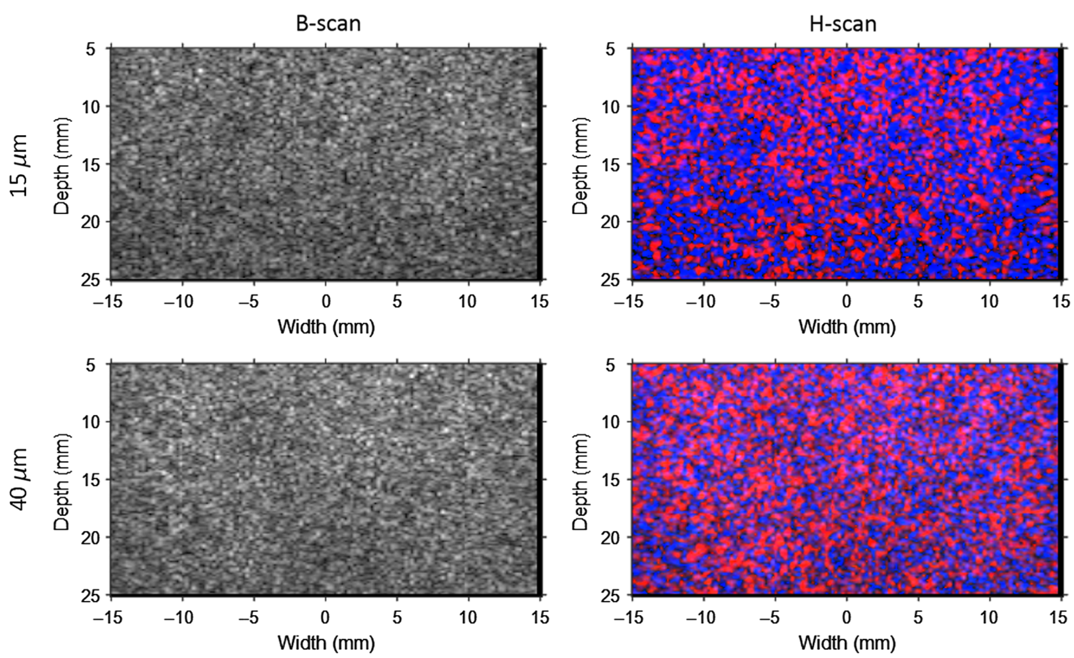

Fig. 3 B-scan and H-scan images of 15- and 40-μm diameter scattering phantoms. The shift in color is due to relative enhancement of the red (**G**$H2$) channel output, as predicted by theory in Fig. 2.

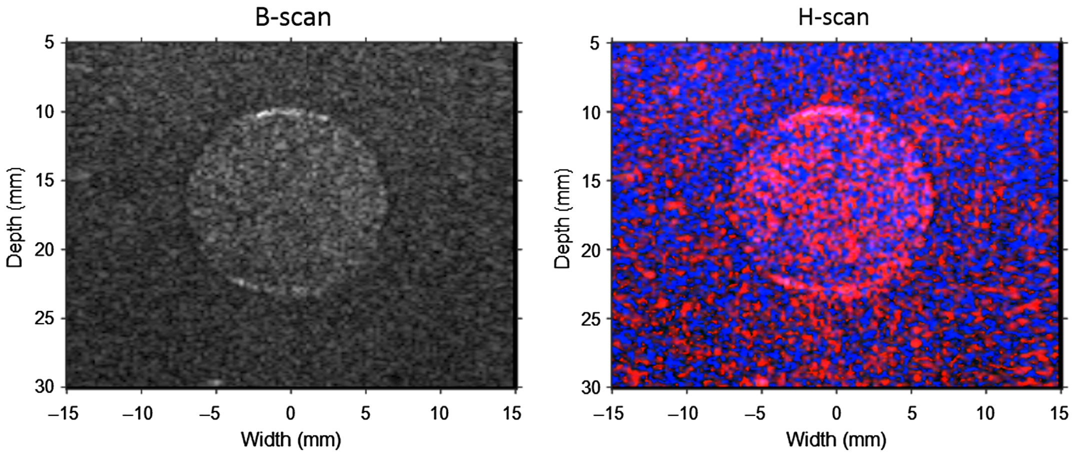

Fig. 4 Inclusion phantom demonstrating a shift in color within the inclusion due to the scattering behavior of the larger (30 μm) diameters relative to the background (15-μm diameters).

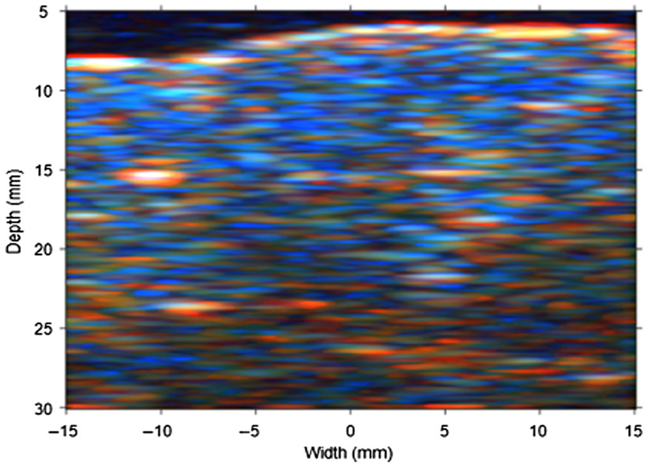

Fig. 5 H-scan of beef liver after soaking in isotonic solution for 24 h.

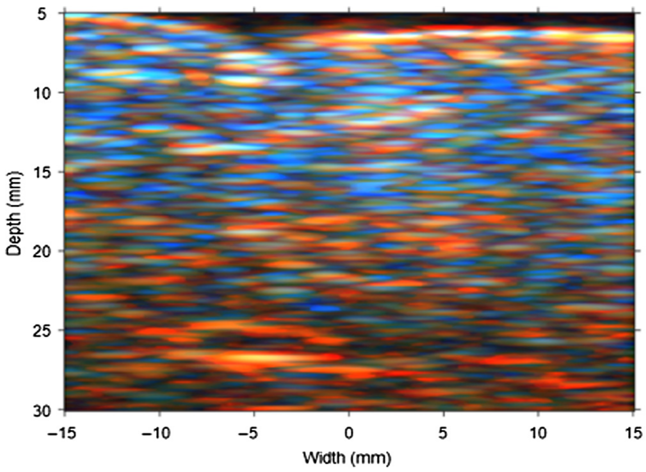

Fig. 6 H-scan of beef liver after soaking in hypotonic solution for 24 h.

than 2 cm^2, the standard error of the means among scan planes within any phantom was <2 dB.

Liver results showed a color shift in the hypotonic liver sections (>10% volume increase after 24 h in cold soak) as compared to isotonic liver sections (~5% volume increase after 24 h in cold soak). The H-scan results are given in Figs. 5 and 6, and a bar chart showing average dB levels for the H-scan channels is shown in Fig. 7. The interpretation of the color shift is plausibly lined to the hypotonic swelling of hepatocytes and other structures; however, there are a number of different structures all contributing to the liver internal echoes, as outlined in Figs. 8 and 9 and in Table 1. We hypothesize that swelling of hepatocytes may also lead to "squeezing" of the smaller sinusoidal fluid channels, thus a number of effects are present simultaneously. Further research is required with advanced morphological assessments to quantify these effects at the micron scale. For now, the point is that relatively subtle changes in tissue scattering sizes can be appreciated as color shifts in the H-scan analysis.

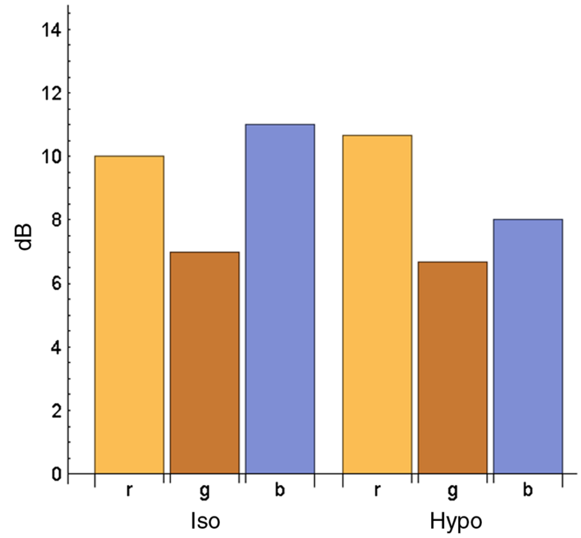

Fig. 7 Comparison of the three channel outputs (**G***H*2, envelope, and **G***H*8, assigned as r, g, b respectively) in dB for the two different conditions: isotonic and hypotonic. Standard error of the means across different scan planes was ±2 to 3 dB. Since the echoes return from a variety of structures (see Table 1), the interpretation must account for the changes across a number of scattering types.

Fig. 8 Photographic images of a liver specimen (a) before and (b) after 24-h soaking in hypertonic solution. Although the sample volume shrinks by 5% to 10%, the diameter of the major vessels appears to remain unchanged or nearly so.

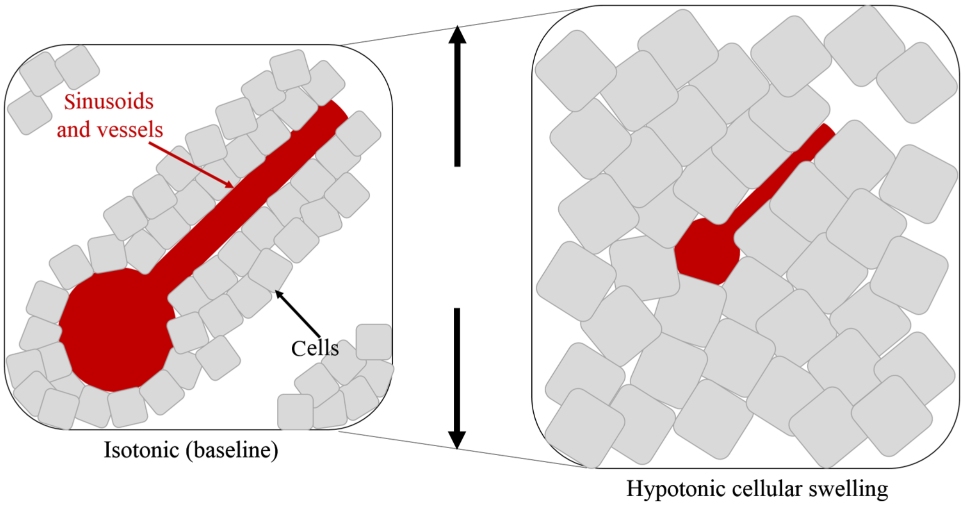

Fig. 9 Schematic of presumed changes in cell size and smaller fluid channel size under two different conditions: after 24-h soaking in hypotonic or isotonic solution. The postulated scattering effects are summarized in Table 1.

Table 1 Changes in structures and scattering following hypotonic conditions, *ex vivo*. The **G***Hn* designation represents the most likely matched filter for each structure based on its size and assuming a **G***H*4 transmit pulse.

	Structure				
Condition	Major arterial walls ligaments (**G***H*4)	Terminal arterial walls (**G***H*5)	Veins and venules (**G***H*6)	Hepatocyte cells (**G***H*6)	Sinusoidal space (**G***H*6)
Isotonic	baseline	baseline	baseline	baseline	baseline
Hypotonic	relatively unchanged	relatively unchanged	decreased radius	increase in size; decreased $\Delta \mathbf{Z}$	decrease in diameter

5 Discussion and Conclusion

The overall results of Sec. 2 demonstrate that H-scan sensitivity to scatterer size is sufficient to visualize differences in subwavelength scatterer size in increments of 10 to 15 μm (radius) using a conventional broadband transducer with a center frequency of 6 MHz. However, it must be noted that the results in Fig. 2 are not an absolute upper limit on sensitivity. First, these results are based on Eqs. (3)–(15) following classical Rayleigh backscatter from a spherical weak scatterer. However there is, in theory, a formulation of average differential backscatter using a modified Gaussian autocorrelation function, proposed in Ref. 13 (see Chapter 8) and more fully developed by Waag et al.[22] [see their Eqs. (11) and (12)] and also in Ref. 23. This function produces a long wavelength limit that includes a higher power law dependence on radius and frequency than the classical Rayleigh result. In fact, Waag has noted average differential scattering cross-section per unit volume measurements with frequency dependences nearing frequency to the fifth power in certain scattering configurations (see Fig. 6 of Ref. 24), and it should be noted that these results are measured in terms of ensemble averages and intensity variables (pressure squared). Thus, Waag proved that it is possible that for a particular configuration of scatterers, a frequency dependence of higher than f^4 for intensity (f^2 for envelope) is possible. In the H-scan analysis, such scatterers would increase the discrimination between $\mathbf{G}Hn$ channels by a change in leading terms in Eq. (7) and then propagating through Eq. (15). Second, as the bandwidth of transducers increases, the adjustment of the $\mathbf{G}Hn$ channels is possible, leading to less overlap between Hermite spectra. These factors can modify the results of Eq. (15) and Figs. 1 and 2, thus they should not be construed as absolute upper limits.

In practice, there are depth-dependent effects that could influence the H-scan analyses. Attenuation and focusing are two potential influences on the H-scan channel outputs. Attenuation is frequency dependent in tissues, so the higher frequencies (corresponding to the $\mathbf{G}H8$ or blue channel in this analysis) are more strongly diminished as a function of depth. As an example of this effect, the phantom shown in Fig. 3(a) comprised of 15-μm scatterers was subdivided into thirds by depth, and the ratio of the average B envelope to average R envelope was computed for each zone. Compared to the middle ROI, the upper third (proximal) was found to have 7% higher B/R, and the lower third (distal) was found to have 15% lower B/R ratio, indicating a progressively weaker B channel output (relative to the R channel output) with depth. This progressive relative loss of the higher frequencies is a natural consequence of frequency-dependent attenuation, which could be more pronounced in some tissues compared to this phantom. Additional work is required to develop compensation strategies for depth-dependent biases.

Disclosures

No conflicts of interest, financial or otherwise, are declared by the authors.

Acknowledgments

The authors are indebted to Professor Robert Waag for his illuminating explanations of scattering. This work was supported by the Hajim School of Engineering and Applied Sciences, the University of Rochester, National Institutes of Health Grants Nos. K25EB017222 and R21CA212851 and the Cancer Prevention and Research Institute of Texas Award No. RR150010.

References

1. K. J. Parker, “The H-Scan format for classification of ultrasound scattering,” *OMICS J. Radiol.* **5**(5), 1000236 (2016).
2. K. J. Parker, “Scattering and reflection identification in H-scan images,” *Phys. Med. Biol.* **61**(12), L20–L28 (2016).
3. M. Abramowitz and I. A. Stegun, *Handbook of Mathematical Functions with Formulas, Graphs, and Mathematical Tables*, US Government Publishing Office, Washington, DC (1964).
4. A. D. Poularikas, *Transforms and Applications Handbook*, 3rd ed., CRC Press, Boca Raton, Florida (2010).
5. R. C. Waag et al., “Frequency-dependent angle scattering of ultrasound by liver,” *J. Acoust. Soc. Am.* **72**(2), 343–352 (1982).
6. R. C. Waag, “A review of tissue characterization from ultrasonic scattering,” *IEEE Trans. Biomed. Eng.* **BME-31**(12), 884–893 (1984).
7. F. L. Lizzi et al., “Statistical framework for ultrasonic spectral parameter imaging,” *Ultrasound Med. Biol.* **23**(9), 1371–1382 (1997).
8. F. L. Lizzi et al., “Ultrasonic spectrum analysis for tissue assays and therapy evaluation,” *Int. J. Imaging Syst. Technol.* **8**(1), 3–10 (1997).
9. M. L. Oelze, J. F. Zachary, and W. D. O’Brien Jr., “Characterizaion of tissue microstructure using ultrasonic backscatter: theory and technique for optimization using a Gaussian form factor,” *J. Acoust. Soc. Am.* **112**(3), 1202–1211 (2002).
10. T. L. Szabo, *Diagnostic Ultrasound Imaging: Inside Out*, Elsevier Academic Press, Burlington, Massachusetts (2004).
11. J. W. Strutt, “Investigation of the disturbance produced by a spherical obstacle on the waves of sound,” *Proc. London Math. Soc.* **s1–4**(1), 253–283 (1871).
12. L. Rayleigh, “XXXVII. On the passage of waves through apertures in Plane screens, and allied problems,” *Philos. Mag. Ser. 5* **43**(263), 259–272 (1897).
13. P. M. C. Morse and K. U. Ingard, *Theoretical Acoustics*, Princeton University Press, Princeton (1968).
14. M. F. Insana et al., “Describing small-scale structure in random media using pulse-echo ultrasound,” *J. Acoust. Soc. Am.* **87**(1), 179–192 (1990).
15. A. Ishimaru, *Wave Propagation and Scattering in Random Media*, Academic Press, New York (1978).
16. A. Macovski, *Medical Imaging Systems*, Prentice-Hall, Englewood Cliffs, New Jersey (1983).
17. J. L. Prince and J. M. Links, *Ultrasound Imaging Systems*, Pearson Prentice Hall, Upper Saddle River, New Jersey (2006).
18. K. Hoyt, B. Castaneda, and K. J. Parker, “Two-dimensional sonoelastographic shear velocity imaging,” *Ultrasound Med. Biol.* **34**(2), 276–288 (2008).
19. M. Khairalseed et al., “Spatial angular compounding technique for H-scan ultrasound imaging,” *Ultrasound Med. Biol.* (in press).
20. C. B. Burckhardt, “Speckle in ultrasound B-mode scans,” *IEEE Trans. Sonics Ultrason.* **25**(1), 1–6 (1978).
21. R. F. Wagner et al., “Statistics of speckle in ultrasound B-scans,” *IEEE Trans. Sonics Ultrason.* **30**(3), 156–163 (1983).
22. R. C. Waag, D. Dalecki, and W. A. Smith, “Estimates of wave front distortion from measurements of scattering by model random media and calf liver,” *J. Acoust. Soc. Am.* **85**(1), 406–415 (1989).
23. R. C. Waag, D. Dalecki, and P. E. Christopher, “Spectral power determinations of compressibility and density variations in model media and calf liver using ultrasound,” *J. Acoust. Soc. Am.* **85**(1), 423–431 (1989).
24. J. A. Campbell and R. C. Waag, “Ultrasonic scattering properties of three random media with implications for tissue characterization,” *J. Acoust. Soc. Am.* **75**(6), 1879–1886 (1984).

Mawia Khairalseed received his BS degree in biomedical engineering from Sudan University of Science and Technology (SUST) in 2002 and his MS and PhD degrees in biomedical engineering from Cairo University in 2007 and 2011, respectively. He became an associate professor of biomedical engineering at SUST in 2015. He was the head of biomedical engineering at SUST from 2012 to 2016. He joined the Bioengineering Department, UT Dallas, in 2016 as a research associate. His medical imaging research interests include ultrasound imaging and signal processing for biomedical applications.

Kenneth Hoyt is an associate professor at the Department of Bioengineering, the University of Texas at Dallas. He received his BS degree in electrical engineering from Drexel University in 2001 and his MS and PhD degrees in biomedical engineering in 2004 and 2005, respectively, from the same institution. He did a postdoctoral fellowship at the Department of Electrical and Computer Engineering, the University of Rochester. He received the American Institute of Ultrasound in Medicine New Investigator Award in 2010 and was elected fellow in 2014.

Juvenal Ormachea received his BS degree in electronics engineering and his MS degree in digital signal and image processing from the Pontificia Universidad Catolica del Peru in 2011 and 2015, respectively. He also earned his MS degree in electrical engineering from the University of Rochester in 2016, where he is currently pursuing his PhD in electrical and computer engineering.

Alberto Terrazas is a MS student in electronic engineering at the Instituto Tecnológico y de Estudios Superiores de Monterrey, Mexico, where he also earned his BS degree in biomedical engineering. He is a current member of the bioinformatics and medical devices group. He is a consultant in *in vitro* diagnostics for bioMerieux.

Kevin J. Parker, PhD, is the William F. May professor of engineering at the University of Rochester. He earned his graduate degrees from Massachusetts Institute of Technology and served at the University of Rochester as department chair, director of the Rochester Center for Biomedical Ultrasound, and dean of engineering/applied sciences. He holds 25 US and 13 international patents (licensed to 25 companies), is a founder of VirtualScopics, and has published 200 journal articles. He is a fellow of IEEE, AIUM, ASA, AIMBE, and NAI.